

# Bioinspired Geometry-Switchable Janus Nanofibers for Eye-Readable H<sub>2</sub> Sensors

Heetak Han, Sangyul Baik, Borui Xu, Jungmok Seo, Sanggeun Lee, Sera Shin, Jaehong Lee, Ja Hoon Koo, Yongfeng Mei, Changhyun Pang,\* and Taeyoon Lee\*

Nanoscale architectures found in nature have unique functionalities and their discovery has led to significant advancements in various fields including optics, wetting, and adhesion. The sensilla of arthropods, comprised of unique hierarchical structures, are a representative example which inspired the development of various bioinspired systems, owing to their hypersensitive and ultrafast responsivity to mechanical and chemical stimuli. This report presents a geometry-switchable and highly H<sub>2</sub>-reactive Janus nanofiber (H-NF) array inspired by the structural features of the arthropod sensilla. The H-NF array (400 nm diameter, 4 μm height, 1.2 μm spacing distance, and hexagonal array) exhibits reversible structural deformation when exposed to a flammable concentration of hydrogen gas (4 vol% H<sub>2</sub> in N<sub>2</sub>) with fast response times (5.1 s). The structural change can be detected with the bare eye, which is a result of change in the optical transmittance due to the structural deformation of the H-NF array. Based on these results, an eye-readable H<sub>2</sub>-sensor that requires no additional electrical apparatus is demonstrated, including wetting-controllable H<sub>2</sub>-selective smart surfaces and H<sub>2</sub>-responsive fasteners.

## 1. Introduction

The discovery that natural architectures possess extraordinary functionalities has had an impact on virtually every aspect of modern materials science, including adhesion, optics, and wetting.<sup>[1,2]</sup> In particular, the sensilla of arthropods have inspired the

development of highly effective artificial sensors and nano/microactuators, such as protein-responsive nanostructures,<sup>[3]</sup> tactile or flow sensors,<sup>[4]</sup> microrobot antennae,<sup>[5]</sup> and cellular biosensors.<sup>[6]</sup> It is known that the antennae of insects are hypersensitive and have ultrafast response times to various mechanical and chemical stimuli (e.g., tactile touch, heat/flow diffusion, vibration, and olfaction) due to their unique hierarchical fibrous architectures connected to mechano-/chemoreceptive sensory organs.<sup>[7]</sup> In this respect, technological advances have been achieved in highly sensitive sensors with nanoscale morphologies to detect explosive gas or cellular interfaces using the resonant frequency shift of nanostructured microcantilever.<sup>[8,9]</sup> However, certain features of arthropod sensilla, which produce fast response time and microscale actuation based on the reversible mechano-/

chemoreactive bending of the numerous fibrous elements of the antennae, have not yet been integrated into artificial bioinspired devices. Moreover, previously described sensors based on microcantilevers might require complicated microelectromechanical systems techniques so that simple and cost-effective methods for the fabrication of sensilla-like sensors for practical applications remain a challenge.

In addition, the efficient and accurate detection of hydrogen (e.g., in fuel cells and combustion engines) is known to be extremely critical due to the potential hazards that exist even at extremely low atmospheric hydrogen concentrations (>4% H<sub>2</sub> by volume). In general, some conventional hydrogen sensors require electric monitoring that is based on expensive semiconductors, protonic conductors, or platinum wires. Despite their high sensitivity and accuracy, safety precautions to minimize the risk of explosion due to the electric currents in these devices must be implemented. Another type of H<sub>2</sub> sensor based on optical modulations such as the surface plasmon resonance and surface plasmon polaritons of metamaterials would also fall short due to the requirement of expensive optical analyzers and sophisticated read-outs.<sup>[10–12]</sup> On the other hand, eye-readable hydrogen gas sensors have been developed using plasmonic nanostructured metamaterials (e.g., Au–Pd) or hydrogen-reactive chemochromic materials such as Y, CuS, and WO<sub>3</sub>.<sup>[13–15]</sup> However, for the reversible optical monitoring of hydrogen gas, previous Pd-hybridized hydrogen sensors (e.g., WO<sub>3</sub>-Pd)

H. Han, S. Lee, S. Shin, Dr. J. Lee, Prof. T. Lee  
School of Electrical and Electronic Engineering  
Yonsei University  
50 Yonsei-ro, Seodaemun-gu, Seoul 03722, Republic of Korea  
E-mail: taeyoon.lee@yonsei.ac.kr  
S. Baik, J. H. Koo, Prof. C. Pang  
School of Chemical Engineering  
SKKU Advanced Institute of Nanotechnology (SAINT)  
Samsung Advanced Institute for Health Science & Technology (SAIHST)  
Sungkyunkwan University (SKKU)  
Seobu-ro, Jangan-gu, Suwon, Gyeonggi-do 440-746, Republic of Korea  
E-mail: cpang@skku.edu  
B. Xu, Prof. Y. Mei  
Department of Materials Science  
Fudan University  
220 Handan Road, Shanghai 200433, China  
Dr. J. Seo  
Center for Biomaterials  
Korea Institute of Science and Technology  
14 Hwarang-ro, Seongbuk-gu, Seoul 02792, Republic of Korea

DOI: 10.1002/adfm.201701618

showed relatively long response times ( $\approx 10$  min) under atmospheric pressure and room temperature.<sup>[15]</sup> Although excellent performance was reported for an Y-based optical sensor hydrogenated with H<sub>2</sub> gas,<sup>[14]</sup> the fabrication of multiple stacking layers (Y/Pd/PTFE) would be considered to be cumbersome in the realization of a cost-effective device with crack-resistant flexibility. Furthermore, hydrogen-sensitive devices could be evolved into an inexpensive, easily fabricated, and read smart devices with controllable nanoactuators that operate in a flexible and reversible manner.

In this work, we developed a highly sensitive, eye-readable, and flexible hydrogen sensor based on sensilla-inspired H<sub>2</sub>-reactive Janus nanofibers (H-NFs), wherein one side of the nanofiber is coated with a layer of hydrogen-sensing metal (Pd), while the other side is composed of a polymer. We utilized and miniaturized the main structural features of insect sensilla to obtain high sensitivity and fast response time, which originate from the unique properties of the densely populated array of slanted nanofibers. In accordance with their amplified surface areas for ultrasensitivity, H-NF arrays are expected to possess fast response times via an elastic response to the geometry-switchable displacement that arises from the volume change reactions due to the presence/absence of hydrogen molecules on the Janus-faced surfaces of nanofibers. We found the morphologically controllable H-NF array to be highly sensitive, with a maximum sensitivity of  $\approx 65\%$  (sensitivity is defined as the ratio between the change in transmittance and the base transmittance) and fast response time of 5.1 s in response to the presence of a flammable concentration of hydrogen gas (4 vol% H<sub>2</sub> in N<sub>2</sub>; repeatability <40 cycles). Through the straightforward fabrication of sensilla-like nanofibers, we developed a self-powered, highly sensitive, and ultrafast H<sub>2</sub> sensor that allowed simple detection with the naked eye without requiring additional electrical apparatus. Furthermore, we demonstrated that the H-NF array described herein can potentially be employed in wetting-controllable, H<sub>2</sub>-reactive nanoactuators and in hazard-warning devices that use a H<sub>2</sub>-sensitive fastener.

## 2. Results and Discussion

**Figure 1a** presents an image of an ant's antenna (*Camponotus japonicus*) and the corresponding scanning electron microscopy (SEM) images that show the particular hierarchical architecture in detail. The SEM images clearly depict the densely populated and slanted appearance of the sensilla, which are  $\approx 2$   $\mu\text{m}$  in diameter and 20  $\mu\text{m}$  in height (aspect ratio, AR = height/diameter = 10). The fibers respond to various tiny mechanical and chemical stimuli by fast displacements, which are expected to transfer tiny forces to the sensory organs.<sup>[16]</sup> Their functionality is known to be critical to flee from predators and is often used in mating, brooding, swimming, and even in anchoring the arthropod to a substrate. To mimic the unique features of the antennae of ants, we produced an H-NF array, which involved the production of polyurethane acrylate (PUA, MINS 301 RM) nanofibers, followed by the oblique deposition of Pd onto nanofibers by sputter deposition at an incident ion beam angle of 45° (refer to Figure 1b and the Experimental Section). In this paper, we used the PUA having a moderated elastic modulus

( $\approx 20$  MPa) and surface energy ( $\approx 40$  mJ m<sup>-2</sup>) for elastically deforming the nanofibers without collapse or mating between neighboring nanofibers (see details method in the Supporting Information).<sup>[17]</sup> The straightforward fabrication method is advantageous for the fabrication of uniform, large-area, flexible, and face-selectively H<sub>2</sub>-reactive Janus nanofiber arrays that possess high structural fidelity and integrity, as shown in Figure 1c and d ( $2 \times 2$  cm<sup>2</sup> square area; 400 nm diameter nanofibers; AR = 10; hexagonal layout).

To explore the potential application of optical sensors based on H<sub>2</sub>-reactive nanoactuators, we fabricated different hybridized Janus nanofiber arrays by varying the size of nanostructures (100 or 400 nm diameter nanofibers) and the thickness of the Pd overcoats (0, 40, 80, or 120 nm), as shown in the SEM images presented in **Figure 2a** (eight total experimental sets; see the Supporting Information for details). After deposition of the Pd overcoats, the previously upright fibers in the nano/microfiber arrays became slanted. The slanting effect is attributed to fiber degradation caused by the 45° Ar-ion-beam irradiation employed in the Pd deposition process.<sup>[18]</sup> The overall result was sensilla-like, high AR Janus fibers that were highly uniform and coated with a thin Pd layer on the right/concave side of the fibers, as shown in Figure 2a. In addition, by composition (COMPO) mode SEM observation, the right Pd-coated side of the nanofibers appeared significantly brighter than the left PUA side due to strong backscattering from the Pd layer (Figure S1, Supporting Information).<sup>[19]</sup> Finally, as can be seen in Figure 2a,b, slanted nanofiber arrays were created and the extent of the slant, i.e., the bending angle, was strongly related to the coating time/thickness of the Pd layer. In the case of relatively large fiber array (3  $\mu\text{m}$  diameter and 18  $\mu\text{m}$  height), however, there was no notable morphological change after Pd deposition or hydrogen exposure, since the residual stress by asymmetrical Pd deposition (<100 nm) was insufficient to control the geometry due to the high moment of inertia of structures (see Figure S2 in the Supporting Information).

The underlying mechanism for the switchability of the Janus nanofiber is illustrated in Figure 2c. When hydrogen gas is introduced into the asymmetric Pd layer, Pd turns into palladium hydride (PdH<sub>x</sub>) via a reversible surface reaction, resulting in a volume change under atmospheric pressure and room temperature.<sup>[20,21]</sup> Thus, the bending angle of the nanofibers is expected to be switchable in response to the loading/unloading of H<sub>2</sub> due to the expansion/contraction of the Pd overcoat, which is asymmetrically deposited on one side of the nanofibers. This mechanism predicts a shutter-like shadowing effect upon exposure of the H-NF array to H<sub>2</sub> gas, which suggests that the optical transmittance of the H-NF array may be responsive to the H<sub>2</sub> loading/unloading. In Figure 2d, we plotted the optical transmittance changes ( $\Delta T/T_0$ ) as a function of Pd layer thickness for flat Pd/PUA films (Flat Pd layer) and slanted H-NF arrays upon exposure to 4 vol% H<sub>2</sub> in N<sub>2</sub> carrier gas (see the Supporting Information for measurement details). In particular, the sensitivity of the H-NF arrays can be defined as  $S = \Delta T/T_0$ ,<sup>[22]</sup> where  $\Delta T$  is the change in transmittance upon exposure to H<sub>2</sub> and  $T_0$  is the base transmittance under ambient air. Herein, all sensitivity measurements were conducted using 530 nm visible light since the human eye is highly sensitive to green wavelengths (495–570 nm) (see Figure S3 in the Supporting Information).

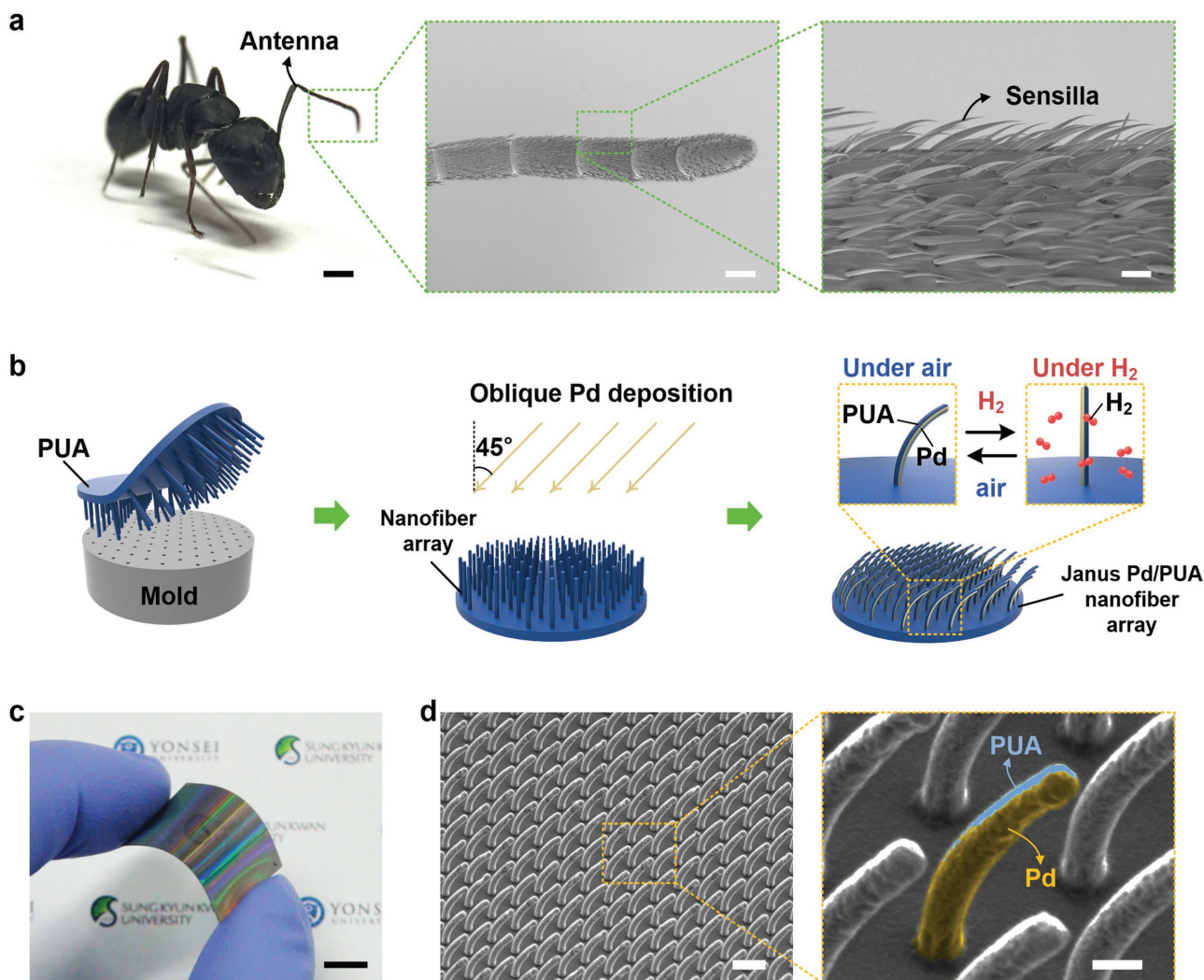


**Figure 1.** a) Photograph of an ant (*Camponotus japonicus*) and SEM images of its antenna composed of high AR ( $\approx 10$ ) slanted sensilla. Scale bars from left to right: 1 mm, 100  $\mu\text{m}$ , and 10  $\mu\text{m}$ . b) Schematic illustration of the H-NF array fabrication procedure. c) Photograph of a flexible and semitransparent H-NF array. Scale bar: 1 cm. d) Low and high magnification SEM images of an H-NF array (400 nm diameter and 100 nm Pd overcoat) with slanted sensilla-like Janus nanofibers. Scale bars from left to right: 2 and 500 nm.

As shown in Figure 2d, nanofibers with 400 nm diameters and 100 nm thick asymmetric Pd coating exhibited the highest difference in light transmittance ( $\approx 65\%$ ) in response to hydrogen gas (4 vol%  $\text{H}_2$  in  $\text{N}_2$ ; 1 atm; room temperature). This behavior is attributed to the nanofiber displacement caused by the force balance between expansion stress and resistance upon reaction with  $\text{H}_2$ , which acts to reduce optical shadowing without incurring delamination of the Pd/Polymer Janus nanofiber. On the other hand, nanofibers with 100 nm diameters showed a similar optical sensitivity to that of the flat Pd film. This may be attributed to the spacing distance between the nanofibers (300 nm for nanofibers with 100 nm diameters), which was even smaller than the measuring wavelength (530 nm). The mechanism underlying the elastic behaviors responsible for the shadowing effect will be discussed in detail later in the paper.

To demonstrate the switchable nature of the structural deformation of the H-NF upon  $\text{H}_2$  exposure, the cross-sectional views of the H-NF array (400 nm diameter nanofibers;

AR = 10; 100 nm thick asymmetric Pd overcoats) were examined, as shown in Figure 2e (i) (10 vol%  $\text{H}_2$  in  $\text{N}_2$ ; 1 atm; room temperature; see Movie S1 in the Supporting Information). Here the bending angle of the nanofiber was initially  $\approx 17.3^\circ$  and rapidly decreased to  $\approx 10.2^\circ$  within 4 s upon  $\text{H}_2$  exposure. After unloading the  $\text{H}_2$  gas, the H-NF returned to its initial state within 6 s (see Figures S4 and S5 in the Supporting Information for side view and top view, respectively). The change in the bending angle ( $\Delta\delta$ ) of the H-NF due to  $\text{H}_2$  gas exposure can be explained by the beam-bending theory regarding geometric features and strain induced by the volume-changeable surface reaction of H-NF,<sup>[23]</sup> which is given by

$$\Delta\delta = -\frac{540ldt}{\pi(d+t)^3} \epsilon_{\text{H}_2} \quad (1)$$

where  $l$  is the nanofiber length,  $d$  is the nanofiber diameter,  $t$  is the thickness of the Pd layer, and  $\epsilon_{\text{H}_2}$  is the strain due to the

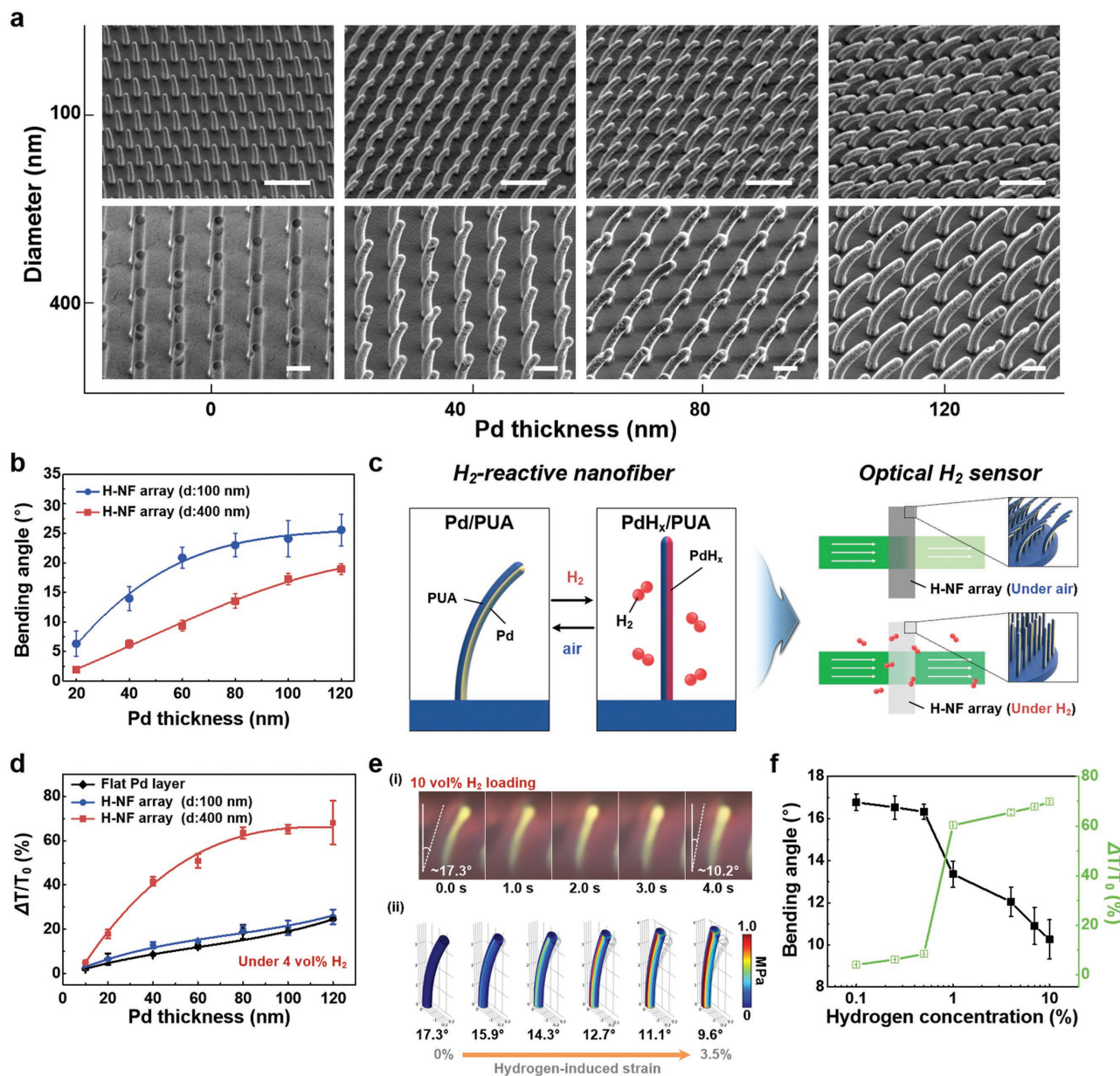


**Figure 2.** a) SEM images of the Janus nanofiber arrays with different nanostructure sizes (nanofiber diameters of 100 or 400 nm) and various thicknesses of asymmetrically deposited Pd overcoats (0, 40, 80, and 120 nm). Scale bars: 1  $\mu\text{m}$ . b) The bending angle of the Janus nanofiber arrays as a function of Pd thickness. Here the bending angle of the nanofiber was defined as the tangential angle at the tip of the nanofiber. c) Schematic showing the underlying mechanism for the reversible morphological deformation and optical transmittance change of the  $\text{H}_2$ -reactive nanofibers in response to the presence of  $\text{H}_2$ . d) Sensitivity ( $S = \Delta T/T_0$ ) of the H-NF-based (nanofiber diameters of either 100 or 400 nm) and flat Pd layer-based devices as a function of Pd thickness. e) (i) Real-time cross-sectional images of the H-NF response to exposure to 10 vol%  $\text{H}_2$  in  $\text{N}_2$ . (ii) Data calculated from finite-element modeling of the lattice expansion of H-NF array under  $\text{H}_2$  (10 vol%  $\text{H}_2$  in  $\text{N}_2$ ). f) Plots of bending angle and sensitivity as a function of  $\text{H}_2$  concentration.

lattice expansion of the Pd overcoat upon  $\text{H}_2$  exposure. The change in strain ( $\epsilon_{\text{H}_2} < 3.5\%$ ) originates from the reversible surface reaction of the Pd overcoat, i.e., generation of  $\text{PdH}_x$  with associated lattice expansion.<sup>[24,25]</sup> Based on our simple model, the maximum bending angle of H-NF is  $\approx 7.7^\circ$ , which is in good agreement with the experimental data presented in Figure 2e(i,ii) (see the Supporting Information for simulation details). In addition, Figure 2f shows the unique  $\text{H}_2$ -reactive behaviors of the

H-NF array, resulting in an eye-readable sensor with reversible transmittance changes across  $\text{H}_2$  concentrations of 0.1–10 vol% in  $\text{N}_2$ . The dramatic change in the bending angle and transmittance at  $\approx 1$  vol%  $\text{H}_2$  in  $\text{N}_2$  is attributed to the relatively large lattice expansion of  $\text{PdH}_x$  due to the phase transition from  $\alpha$  to  $\beta$ .<sup>[24,25]</sup> In other words, the  $\alpha$  phase of  $\text{PdH}_x$  dominates at  $\text{H}_2$  concentrations below 1 vol% wherein lattice expansion ( $\epsilon_{\text{H}_2}$ ) is smaller than 0.13%.

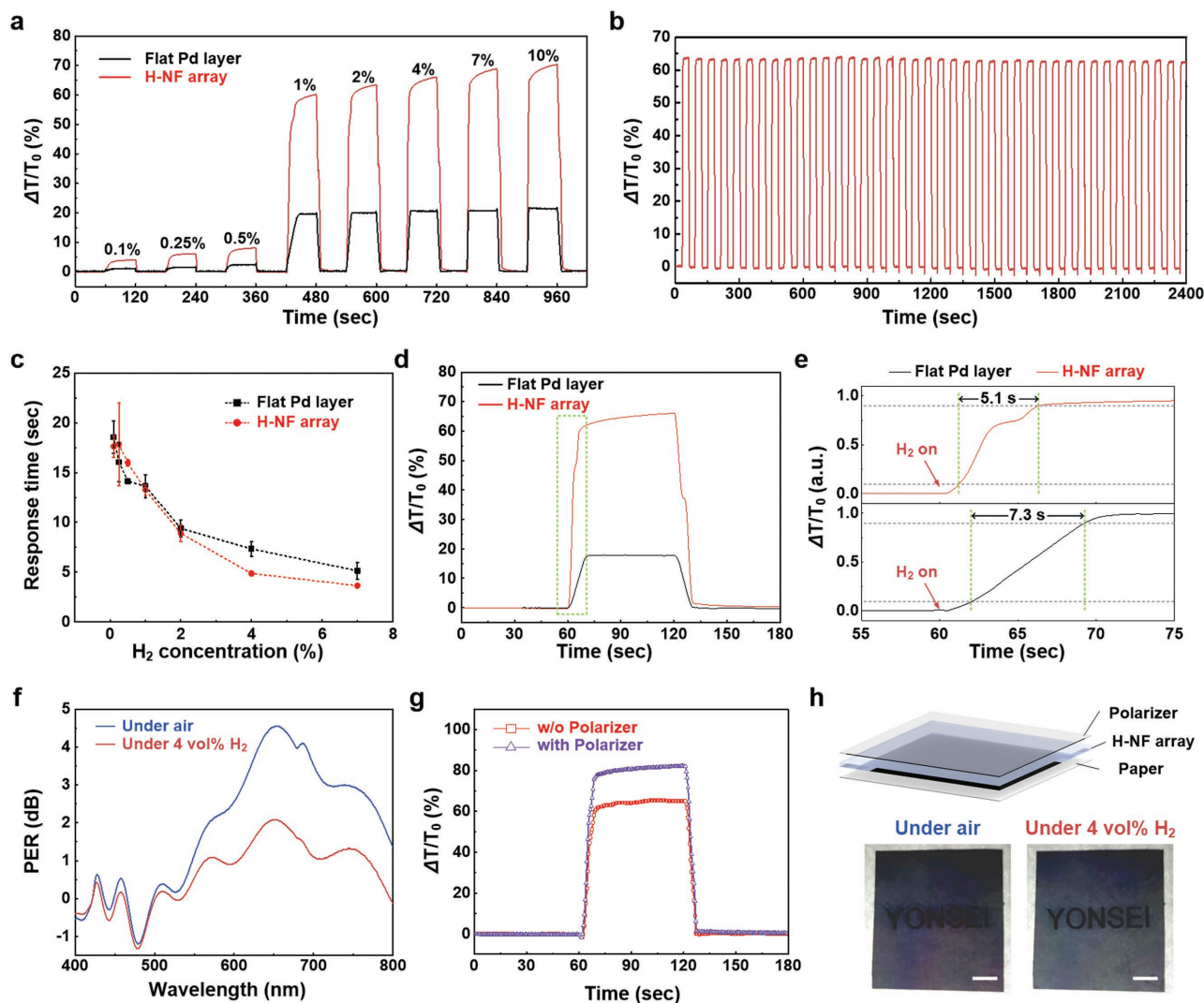


**Figure 3.** a) Real-time on-off behaviors of optical sensors based on an H-NF array (400 nm diameter nanofibers with 100 nm thick asymmetric Pd overcoats) or a flat Pd layer in response to various concentrations of  $H_2$ , ranging from 0.1 to 10 vol%. The atmosphere in the chamber was repeatedly switched between air and  $H_2$  for each cycle after a waiting period of 60 s. b) Repeatability of optical transmittance response of the H-NF array upon loading/unloading 4 vol%  $H_2$  in  $N_2$ . c) Response time of the H-NF array and flat-Pd layer as a function of  $H_2$  concentration. d) Real-time behaviors and e) the response times of the H-NF array and the flat Pd layer upon exposure to 4 vol%  $H_2$  in  $N_2$ . f) PER spectra of the H-NF array under air and 4 vol%  $H_2$  in  $N_2$  carrier gas. g) The on-off behaviors of the H-NF array with and without a polarizer in the direction perpendicular to the nanofiber bending direction in response to the presence of 4 vol%  $H_2$  in  $N_2$ . h) Schematic of the eye-readable  $H_2$  detection system, and images showing the polarizer combined H-NF array based eye-readable sensor under air and 4 vol%  $H_2$  in  $N_2$  atmosphere. Scale bars: 2 mm.

To investigate the on-off behaviors of an optical sensor based on the H-NF array (400 nm diameter nanofibers; AR = 10; 100 nm thick asymmetric Pd overcoats), we measured the transmittance in response to various concentrations of  $H_2$  ranging from 0.1 to 10 vol%, as shown in **Figure 3a** (see the Supporting Information for details). The optical sensitivity of the H-NF-based device was significantly better compared with that of the flat Pd-layered device, which required an additional apparatus (e.g., a light detector and display) and often suffered delamination between the Pd overcoat and the substrate.<sup>[26,27]</sup> In addition, the optical response of the H-NF array was stable during multiple cycles (<40 cycles) without any notable degradation as shown in **Figure 3b** (see the Supporting information for the detailed method). As shown in **Figure 3c**, the response

times of H-NF array were decreased from 17.6 to 3.6 s as increasing  $H_2$  concentration (0–7 vol%  $H_2$  in  $N_2$ ). In particular, the H-NF-based sensor showed faster response time (5.1 s) than those of flat Pd-layer upon flammable hydrogen concentration (4 vol%  $H_2$  in  $N_2$  carrier gas) due to the resilience of the PUA nanofiber which can help the recovery of bent nanofibers (see **Figure 3d,e**). Here, the response time was defined as the time required for the transmittance to change from 10% to 90%.

To explain the optical behavior of the H-NF-based sensor, we developed a simple theory of optical nano-shutters that underlies the switchable motions of the H-NF array. For a hexagonal unit cell array of slanted nanofibers with a spacing ratio (SR = distance between the nanofibers (s)/diameter of nanofiber (d)) of 3, the area of the unit cell can be divided into two

regions: (i) the shaded region and (ii) the unshaded region (see Figure S6 in the Supporting Information). The transmittance of an H-NF array ( $T = \Phi^t/\Phi^i$ ; the transmitted radiation flux divided by the incident flux) with shaded and unshaded regions can be explained according to the well-known phenomena of directional transmittance. In addition, the total transmitted radiation flux ( $\Phi^t$ ) is the sum of the transmitted radiation flux from the shaded region ( $\Phi_s^t$ ) and from the unshaded region ( $\Phi_u^t$ ) ( $\Phi^t = \Phi_s^t + \Phi_u^t$ ). Here,  $\Phi_s^t$  is negligible due to the shadowing effect of the H-NF array (the Beer–Lambert law) and the transmittance of the H-NF array can be obtained as  $T \approx T_{Pd} \dot{c} (A_u/A_t)$  (see the Supporting Information for details).  $T_{Pd}$  is the transmittance through the Pd coats,  $A_u$  is the surface area of the unshaded region, and  $A_t$  is the total area of the unit cell. After plugging in the bending angle ( $\delta$ ) with algebraic manipulation, we obtain

$$T_{H_2} \approx T_{Pd,H_2} \left( 0.52 + \frac{3.63ldt}{(d+t)^3} \epsilon_{H_2} \right) \quad (2)$$

where  $T_{Pd,H_2}$  is the transmittance of the flat Pd layer after hydrogen exposure. Our model predicted the transmittance of the H-NF array in response to the hydrogen exposure in terms of the relationship between and geometric parameters and the strain induced by concentrations of  $H_2$  gas, yielding results that are in excellent agreement with experimental observations (see Figure S7 and the Supporting Information for detailed derivation). Based

on the underlying mechanism, the H-NF-based sensor undergoes a polarization effect due to the uniform directionality of the nanofibers, resulting in a polarization extinction ratio (PER) level of  $\approx 4.5$  ( $PER = 10 \log_{10}(T_y/T_x)$ ; see Figure 3f and the Supporting Information for details). Here  $T_x$  and  $T_y$  correspond to the intensity of the light transmitted through a perpendicular polarizer in the  $x$  and  $y$  directions, respectively (see the Supporting Information). Conversely, the flat Pd layer-based device had a nearly zero PER level (Figure S8, Supporting Information). As shown in Figure 3f, the PER of the H-NF array changed with the loading and unloading of  $H_2$  gas due to the switchable motions of the nanofibers. The sensitivity of the H-NF array was improved from 65% to  $\approx 80\%$  at 4 vol%  $H_2$  in  $N_2$  with the aid of a commercial polarizer perpendicular to the bending direction of the nanofiber array as shown in Figure 3g. These enhancements improve the accuracy of naked-eye reads (see Figure 3h, Figure S9, Movie S2, and the Supporting Information for detailed method).

For further potential applications, we also demonstrated a wetting-controllable surface using  $H_2$ -reactive actuation based upon the H-NF array. Recently, directional and controllable wetting studies that rely on asymmetric nanostructures have been proposed for various potential applications such as water collection and micro-biochips.<sup>[28,29]</sup> The H-NF array can be expected to favor the unidirectional spreading because of the slanted nanofiber surface features, as shown in previous works.<sup>[28]</sup> However, bidirectional wetting was observed when the array was exposed to hydrogen gas (4 vol%  $H_2$  in  $N_2$ ), as shown in Figure 4a,b (see green arrows and orange arrows) and Movie S3

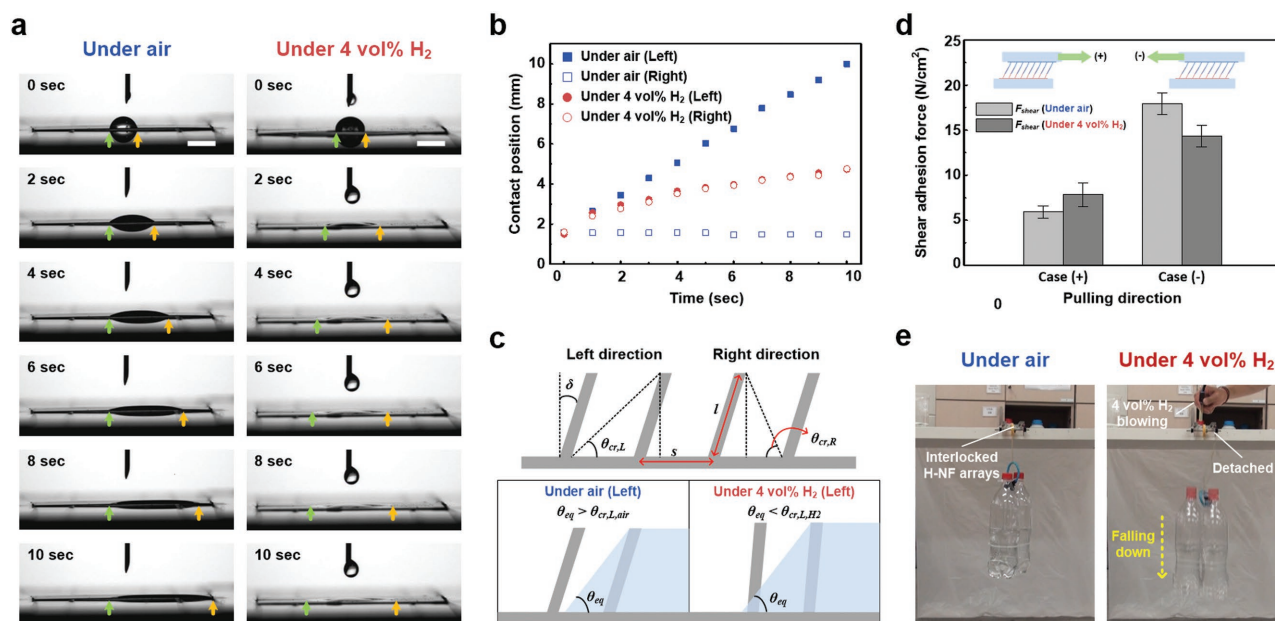


**Figure 4.** a) Real-time side view images of the spreading behaviors of water-based liquid drops on the H-NF array exposed to either air or 4 vol%  $H_2$  in  $N_2$ . Green and orange arrows indicate the left and the right contact lines of the liquid, respectively. Scale bars: 3 mm. b) The position of the left and right contact lines of the liquid on the H-NF array as a function of the elapsed time. The contact line of water-based liquids was defined as the distance from the center of the liquid at 0 s to the edge of the droplet. c) Schematic explaining the underlying mechanism for the change of the liquid wetting behaviors of the H-NF array. The  $\theta_{cr}$  has different values based upon direction and ambient conditions. d) Shear adhesion forces of the interlocked H-NF arrays (100 nm diameter nanofibers with 40 nm thick asymmetric Pd overcoats) with respect to pulling direction and atmospheric conditions. Insets show the different directional adhesions. e) Snapshots of the interlocked H-NF arrays before and after loading of 4 vol%  $H_2$  in  $N_2$  by blowing. Under air, the 1.6 kg object (15.7 N) was supported by the interlocked H-NF arrays. However, after blowing on the arrays with 4 vol%  $H_2$  in  $N_2$ , the object fell due to weakened shear adhesion forces.

(see the Supporting Information for detailed method). These different motions of the aqueous liquids can be understood in terms of the substantial variations in the critical angle ( $\theta_{cr}$ ) for liquid wetting that originates from the actuating nanofibers, as shown in Figure 4c. Here the critical angle should be equal to or larger than the intrinsic contact angle ( $\theta_{eq} \approx 62^\circ$ ; Figure S10, Supporting Information) for advancement of the liquid contact line.<sup>[30]</sup> In particular, the critical angle for liquid advancement in the right direction ( $\theta_{cr,R}$ ) was larger than the  $\theta_{eq}$  regardless of the change in bending angle of the nanofibers ( $90^\circ$  and  $83^\circ$  under ambient air and  $H_2$  atmosphere, respectively), always resulting in liquid spreading in the right direction. However, the critical angle for liquid advancement in the left ( $\theta_{cr,L}$ ) was only larger than the  $\theta_{eq}$  when exposed to  $H_2$  gas ( $58^\circ$  and  $64^\circ$  under ambient air and  $H_2$  atmosphere, respectively), resulting in a bidirectional spreading behavior upon exposure of  $H_2$  (see Table S1 and the Supporting Information for details). In addition, this particular behavior of the metal-hybridized Janus nanofiber array is potentially suitable for  $H_2$ -selective applications due to exclusiveness to other gases of the mechanical bending of the H-NF array.

Furthermore, we developed a fast hazard-warning device using an  $H_2$  gas-sensitive fastener with switchable and directional adhesions via the mechanical interlocking of the slanted Janus nanofiber arrays. As demonstrated in previous reports, stable and reversible shear adhesion forces can be expected by overlapping two identical slanted nanofiber arrays in the opposite directions.<sup>[17,18]</sup> Figure 4d shows the bidirectional, asymmetric interlocking adhesions between slanted, high AR Janus nanofibers utilizing actively geometry-tunable behaviors by the surface reaction between  $H_2$  and the Pd overcoats. Here the shear adhesion forces were measured in the angled (+) and reverse (-) directions with respect to the initial bending geometry, as shown in Figure 4d inset (see also Figure S11 and the Supporting Information for measurement details). In the case of interlocking between slanted nanofiber arrays under conditions of ambient air, the measured shear locking force was  $5.9 \text{ N cm}^{-2}$  in the (+) direction and  $17.9 \text{ N cm}^{-2}$  in the (-) direction, with an adhesion hysteresis of  $\approx 3.0$ . In comparison, the force between  $H_2$ -reacted nanofibers was  $7.9 \text{ N cm}^{-2}$  in the (+) direction and  $14.3 \text{ N cm}^{-2}$  in the (-) direction, with an adhesion hysteresis of  $\approx 1.8$ . These  $H_2$ -switchable adhesion differences can be explained according to a well-established theory based on the competition between van der Waals-mediated interlocking and the angular displacements ( $\Delta\delta$ ) of the H-NF arrays.<sup>[18]</sup> By employing these switchable properties of the H-NF array, we demonstrated a novel hazard-warning fastener wherein the H-NF arrays are fastened and able to support certain weights in an ambient air environment but quickly and controllably unfasten and drop the weights in the presence of flammable levels of  $H_2$  gas (4 vol%  $H_2$  in  $N_2$ ), as shown in Figure 4e (see also Movie S4 in the Supporting Information).

### 3. Conclusion

In summary, we have presented a highly  $H_2$ -reactive, flexible, and simply fabricated geometry-switchable Janus nanofiber array inspired by the structural features of arthropod sensilla. Our experimental and theoretical studies indicate that the

bending angle of the H-NF array is switchable due to structural deformations of the polymeric fibers and the asymmetrically deposited Pd overcoats, resulting in outstanding sensitivity ( $S > 65\%$ ) and fast response time (5.1 s) with stable repeatability ( $< 40$  cycles) for the detection of flammable concentrations of hydrogen gas (4 vol%  $H_2$  in  $N_2$ ). The extraordinary performance of the H-NF array was further improved to enable an eye-readable  $H_2$ -sensor by combination with a polarizer in a straightforward and cost-effective manner. Furthermore, we demonstrated that the applications of our H-NF arrays can be evolved to include wetting-controllable,  $H_2$ -selective smart surfaces, and real-time monitoring via  $H_2$ -detectable fasteners.

### 4. Experimental Section

Detailed experimental procedures are available in the Supporting Information. PUA prepolymers (PUA MINS 311 RM) purchased from the Minuta Tech, Korea, were dispensed onto a master mold and a polyethylene terephthalate (PET) film (50  $\mu\text{m}$ ) was pressed lightly against the liquid drop for it to be used as a supporting backplane. The polymer replica was prepared by UV exposure and additional UV-curing was employed once the mold was removed to complete the process. For the fabrication of the nanofiber arrays, two types of nanoscale fiber structures were prepared from the polymer material: (i) 100 nm diameter nanofibers with 1  $\mu\text{m}$  height, and (ii) 400 nm diameter nanofibers with 4  $\mu\text{m}$  height. Next, the as-fabricated PUA nanofiber array was placed on an inclined holder at an angle of  $45^\circ$  and a Pd layer was deposited vertical to the stage by a DC magnetron sputtering deposition system under high vacuum at  $5 \times 10^{-5}$  Torr. Thus, the Pd was obliquely deposited onto only one side of the PUA nanofibers, resulting in a Janus Pd/PUA nanofiber array.

### Supporting Information

Supporting Information is available from the Wiley Online Library or from the author.

### Acknowledgements

This work was supported by the Priority Research Centers Program (2012-0006689) through the National Research Foundation (NRF) of Korea funded by the Ministry of Education, Science and Technology (MEST) and Mid-Career Researcher Program through NRF grant funded by the MEST (2014R1A2A2A09053061), and the R&D program of MOTIE/KEIT [10064081, Development of fiber-based flexible multimodal pressure sensor and algorithm for gesture/posture-recognizable wearable devices]. We gratefully acknowledge partial support from the National Research Foundation of Korea (NRF-2017K2A9A2A06013377, NRF-2017M3A7B4049466, NRF-2014R1A1A1007162, and NRF-2016H1A2A1908670). This material is also based upon work supported by the Ministry of Trade, Industry & Energy (MOTIE, Korea) under Industrial Technology Innovation Program. No. 10062694, 'Development of nano-materials hybrid fibers and bio-signal sensors for safety underwears of heavy workers'. This work also supported by the Natural Science Foundation of China (Nos. 51322201 and U1632115). In addition, the authors thank Tanaka Kikinokogyo K.K. for comments on the usage and properties of palladium. The Acknowledgements and Figure 1 were updated on August 4, 2017, following initial online publication.

### Conflict of Interest

The authors declare no conflict of interest.

## Keywords

actuators, biomimetics, hydrogen sensors, Janus nanofibers, sensilla

Received: March 28, 2017

Revised: May 1, 2017

Published online: June 30, 2017

- 
- [1] G. Zan, Q. Wu, *Adv. Mater.* **2016**, *28*, 2099.
- [2] N. Zhao, Z. Wang, C. Cai, H. Shen, F. Liang, D. Wang, C. Wang, T. Zhu, J. Guo, Y. Wang, X. Liu, C. Duan, H. Wang, Y. Mao, X. Jia, H. Dong, X. Zhang, J. Xu, *Adv. Mater.* **2014**, *26*, 6994.
- [3] E. C. Yusko, J. M. Johnson, S. Majd, P. Prangkio, R. C. Rollings, J. Li, J. Yang, M. Mayer, *Nat. Nanotechnol.* **2011**, *6*, 253.
- [4] L. Patanè, S. Hellbach, A. F. Krause, P. Arena, V. Dürr, *Front. Neurobot.* **2012**, *6*, 1.
- [5] S. B. Fuller, A. Sands, A. Haggerty, M. Karpelson, R. J. Wood, presented at *2013 IEEE Inter. Conf. Robotics and Automation (ICRA 2013)*, Karlsruhe, Germany, May **2013**.
- [6] B. Kong, J. Tang, Z. Wu, C. Selomulya, H. Wang, J. Wei, Y. Wang, G. Zheng, D. Zhao, *NPG Asia Mater.* **2014**, *6*, e117.
- [7] A. Alfadhel, J. Kosel, *Adv. Mater.* **2015**, *27*, 7888.
- [8] D. Spitzer, T. Cottineau, N. Piazzon, S. Josset, F. Schnell, S. N. Pronkin, E. R. Savinova, V. Keller, *Angew. Chem., Int. Ed.* **2012**, *51*, 5334.
- [9] D. Ramos, J. Mertens, M. Calleja, J. Tamayo, *Sensors* **2007**, *7*, 1757.
- [10] N. Liu, M. Mesch, T. Weiss, M. Hentschel, H. Giessen, *Nano Lett.* **2010**, *10*, 2342.
- [11] R. Jiang, F. Qin, Q. Ruan, J. Wang, C. Jin, *Adv. Funct. Mater.* **2014**, *24*, 7328.
- [12] C. Perrotton, R. J. Westerwaal, N. Javahiraly, M. Slamán, H. Schreuders, B. Dam, P. Meyrueis, *Opt. Express* **2013**, *21*, 382.
- [13] M. E. Nasir, W. Dickson, G. A. Wurtz, W. P. Wardley, A. V. Zayats, *Adv. Mater.* **2014**, *26*, 3532.
- [14] P. Ngene, T. Radeva, M. Slamán, R. J. Westerwaal, H. Schreuders, B. Dam, *Adv. Funct. Mater.* **2014**, *24*, 2374.
- [15] Y. A. Lee, S. S. Kalanur, G. Shim, J. Park, H. Seo, *Sens. Actuators, B* **2017**, *238*, 111.
- [16] T. A. Keil, R. A. Steinbrecht, *Insect Ultrastructure*, Vol. 2 (Eds: R. C. King, H. Akai), Springer, Boston, MA, US **1984**, p. 477.
- [17] C. Pang, T. Il Kim, W. G. Bae, D. Kang, S. M. Kim, K. Y. Suh, *Adv. Mater.* **2012**, *24*, 475.
- [18] C. Pang, S. M. Kim, Y. Rahmawan, K. Y. Suh, *ACS Appl. Mater. Interfaces* **2012**, *4*, 4225.
- [19] D. Kaczmarek, *Scanning* **1997**, *19*, 310.
- [20] J. Seo, S. Lee, H. Han, H. B. Jung, J. Hong, G. Song, S. M. Cho, C. Park, W. Lee, T. Lee, *Adv. Mater.* **2013**, *25*, 4139.
- [21] M. Khanuja, B. R. Mehta, P. Agar, P. K. Kulriya, D. K. Avasthi, *J. Appl. Phys.* **2009**, *106*, 093515.
- [22] S. Yurish, *Modern Sensors, Transducers and Sensor Networks*, Vol. 1, IFSA Publishing, Barcelona, Spain **2012**.
- [23] C. H. Hsueh, *J. Appl. Phys.* **2002**, *91*, 9652.
- [24] T. Xu, M. P. Zach, Z. L. Xiao, D. Rosenmann, U. Welp, W. K. Kwok, G. W. Crabtree, *Appl. Phys. Lett.* **2005**, *86*, 1.
- [25] J. S. Noh, J. M. Lee, W. Lee, *Sensors* **2011**, *11*, 825.
- [26] E. Lee, J. Min, E. Lee, J. Noh, J. Hyoun, B. Jung, W. Lee, *Thin Solid Films* **2010**, *519*, 880.
- [27] W. E. Vargas, I. Rojas, D. E. Azoifeifa, N. Clark, *Thin Solid Films* **2006**, *496*, 189.
- [28] K.-H. Chu, R. Xiao, E. N. Wang, *Nat. Mater.* **2010**, *9*, 413.
- [29] M. J. Hancock, K. Sekeroglu, M. C. Demirel, *Adv. Funct. Mater.* **2012**, *22*, 2223.
- [30] X. M. Yang, Z. W. Zhong, E. Q. Li, Z. H. Wang, W. Xu, S. T. Thoroddsen, X. X. Zhang, *Soft Matter* **2013**, *9*, 11113.